Computational Clues for a New Mechanism in the Glycosylase Activity of the Human DNA Repair Protein hOGG1. A Generalized Paradigm for Purine-Repairing Systems?

Matteo Calvaresi, Andrea Bottoni,* and Marco Garavelli*

Dipartimento di Chimica "G. Ciamician", Universita' di Bologna, via Selmi 2, 40126 Bologna, Italy

Received: February 26, 2007

A theoretical density functional theory (DFT, B3LYP) investigation has been carried out on the catalytic cycle responsible for the glycosylase activity of the human DNA repair protein hOGG1: enzyme activation, cleavage of the glycosidic bond, and expulsion of the damaged base. An unprecedented large quantum mechanics (QM) model system has been used, which includes a complete oxoG molecule, the deoxyribose ring bonded to the phosphate groups, and most of the surrounding residues that simulate the protein binding pocket. It has been found that Asp268 does not play any role in Lys249 activation and that the oxoG basis acts as a coenzyme, triggering nucleophile activation by Lys249 deprotonation. An S_N2 nucleophilic attack by Lys249 on the anomeric carbon then follows. This is the rate-determining step of the process with an activation barrier of 16.7 kcal mol^{-1} in good agreement with the experimental value of 17.1 kcal mol^{-1}. The expelled oxoG plays again as an enzyme cofactor at the end of the process by activating (via proton transfer) ribose ring opening and Schiff base formation. This study suggests a recurring catalytic strategy in the enzymatic cleavage of purine nucleoside where the activation of the leaving group by protonation of the nucleoside base (via an enzymatic general acid) triggers the cleavage of the glycosidic bond.

1. Introduction

Reactive oxygen species (ROS, including O_2^-, H_2O_2, and OH^-)[1] and, in general, organic free radicals[2−4] are responsible of dangerous oxidation processes that target the cellular genome. These powerful oxidants can either form as intermediates in normal cellular metabolism[5] or be generated by external factors such as an ionizing radiation (for instance, UVA exposure through sunlight) or tar and tobacco smoke.

One of the most important and serious ROS-induced damages of the cellular genome is the oxidation of the guanine (G) base in DNA leading to 7,8-dihydro-8-oxoguanine (oxoG, see Scheme 1).[1,6] This process is responsible for a permanent alteration of the DNA base sequence: while guanine pairs with cytosine (C) in the Watson−Crick mode and forms a G:C pair, oxoG can pair either with cytosine or with adenine (A) in the Hoogsteen mode giving rise to an oxoG:A pair. This erroneous pair produces, in the subsequent replication step, a G:C → T:A transversion, one of the most frequent somatic mutations in human cancer.[7]

To avoid the loss of information stored in DNA, due to incorrect replication, a complex cellular defense system against oxoG mutagenesis or other single-base lesions in DNA has evolved. This system, which includes a large ensemble of repair proteins,[8−10] has been extensively investigated either in bacteria or in eukaryotes. These repair proteins are lesion-specific DNA glycosylases that are able to scan the genome searching for damaged base sites and catalyze the breaking of the glycosidic bond linking the base to the DNA backbone.[11−13] These enzymes can be classified into two different groups: (a) mono-functional glycosylases that use an activated water molecule as the catalytic nucleophile and (b) bifunctional DNA glycosylase/β-lyase, where an enzyme residue containing an amine group is the catalytic nucleophile that determines the cleavage of the glycosidic bond and the expulsion of the damaged base, thus generating an enzyme−DNA adduct. In a subsequent step, these enzymes can catalyze the scission of the DNA backbone via a conjugate elimination mechanism (β-lyase activity).

OGG1 (hOGG1 in humans), belonging to this second class, is the eukariotic enzyme that is specifically responsible for the oxoG repair. This enzyme is also a member of a structural super family of mono-functional and bifunctional glycosylases,[14,15] characterized by a helix-hairpin-helix (HhH) element in the active site followed by a Gly/Pro rich loop (HhH-GPD motif) and terminating in an invariant Asp residue (Asp268 in hOGG1).

hOGG1 specifically recognizes the oxoG:C pair and binds the oxidized base in its active site pocket.[2,16−18] Following the most popular mechanistic hypothesis[2] (see Scheme 2), the ϵ-amine group of Lys249, after activation, acts as a nucleophile and attacks the C1 anomeric carbon of the ribose moiety, thus determining the removal of oxoG. The experimental evidence that a mutant form of hOGG1, where Lys249 has been replaced by glutamine, retains substrate recognition but loses the enzyme catalytic activity,[2] supports this mechanistic assumption. The abasic intermediate formed by the initial lysine attack rearranges to a Schiff base. In the following steps, the enzyme can catalyze the cleavage of the DNA strand on the 3′ side of the lesion (β-lyase activity).

Even if several investigations have been carried out during the past decade,[2,19−25] many mechanistic details of the damaged base excision process have not been clarified yet. In particular, the role of the invariant Asp268 has not been completely elucidated. An obvious hypothesis is that this residue can assist the catalytic process by deprotonating the Lys249 amine group and thus augmenting its nucleophilicity. However, Verdine and co-workers have recently demonstrated by mutation experiments[21] that a significant catalytic activity is still present after replacement of Asp268 with amino acids that are not able to

* Corresponding authors. E-mail: marco.garavelli@unibo.it (M.G.) and andrea.bottoni@unibo.it (A.B.).

10.1021/jp071581i CCC: $37.00
Published on Web 05/18/2007

SCHEME 1

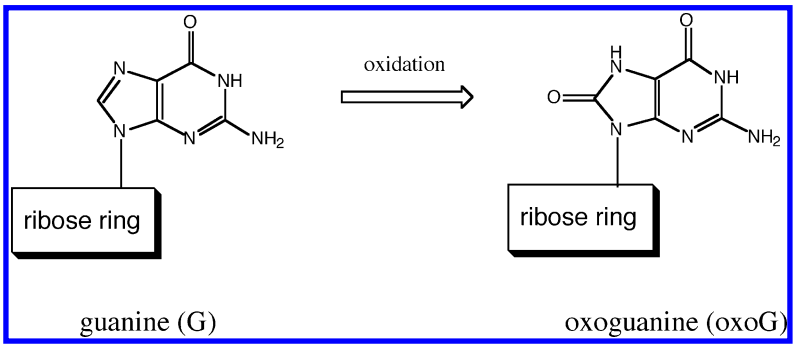

SCHEME 2

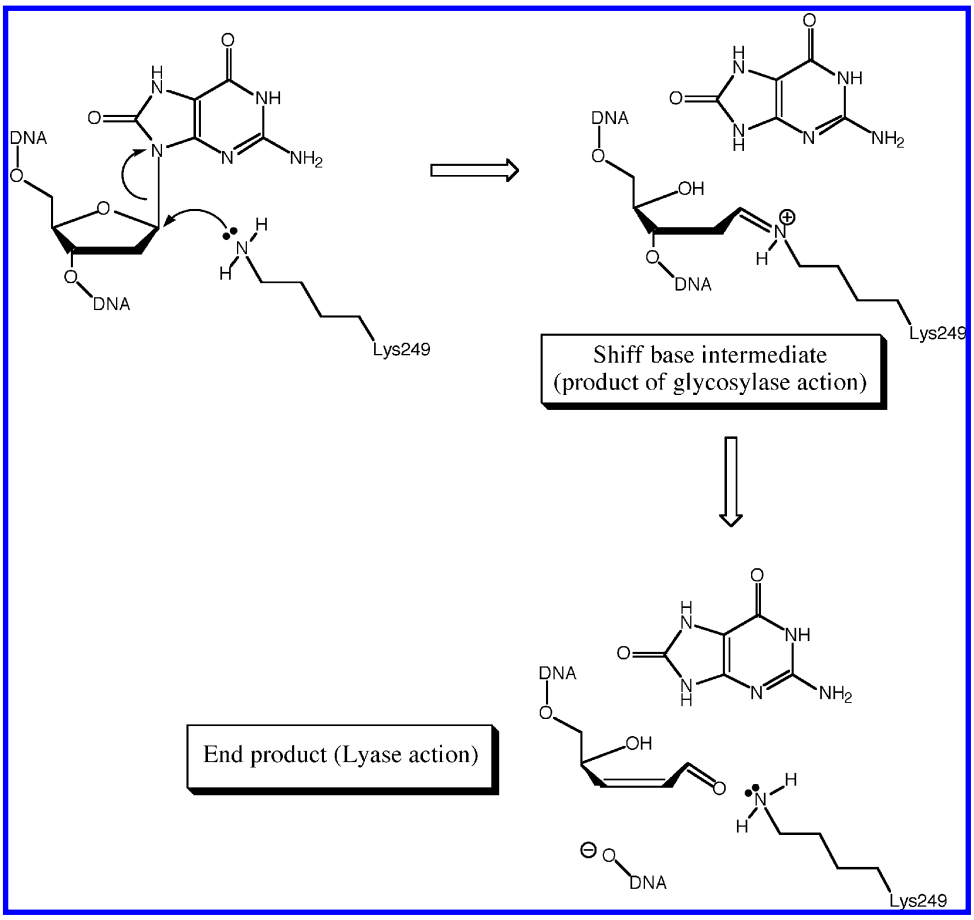

deprotonate the Lys residue. This leads to the conclusion that either Asp268 is not involved in Lys249 deprotonation or a change in the catalytic mechanism occurs in the mutated forms of hOGG1. On the other hand, these experiments show the importance of the Asp268 N-cap interaction (see Scheme 3) in stabilizing the protein fold. This type of intramolecular interaction involves an amino acid side chain at the N-terminal end of an α helix (the aspartate carboxylate group in our case) and one or more protons of the amide groups located along the first turn of the helix (see Scheme 3).

Interestingly, against the possibility that Asp268 assists base excision by deprotonating Lys249, Verdine and co-workers[21] outline the fact that an Asp residue acting as a helix cap should be less basic than a typical aspartate by several orders of magnitude. Also, this stabilizing capping interaction should be completely destroyed to allow Asp268 to approach Lys249. A further important point is provided by the crystal structure of wild hOGG1 bound to a "mutant" substrate (a DNA containing

SCHEME 3

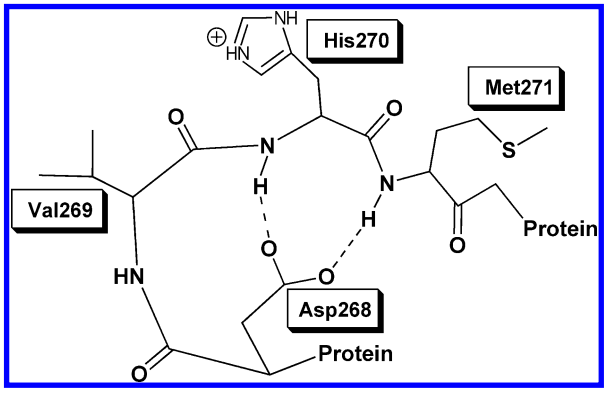

the abasic tetrahydrofuranyl THF moiety and not able to perform catalysis). In this structure, it is evident that Asp268 is not hydrogen bonded to Lys249 as one could expect in the case of an incipient proton transfer involving the two residues. The

possibility of a high energy conformer of hOGG1, where the proton abstraction becomes possible, is not ruled out by these researchers. However, they point out that this hypothesis is not really essential since a slight lowering of the Lys249 pK_a (due to local enzyme microenvironment) would allow the presence of enough neutral amine to carry out base excision.[21] An alternative hypothesis suggested by these structural investigations is that Asp268 stabilizes the positive charge developing on the deoxyribose fragment in the base excision transition state.

An interesting aspect is evidenced by the crystal structure of wild hOGG1 with the THF inhibitor:[19] in the active site, the Lys249 residue is oriented toward C1 with the amine group well-positioned for a nucleophilic attack (distance of 3.5 Å), suggesting an S_N2 process. Anyway, on the basis of the crystallographic structure of a substrate bound mutated form (D268N) of hOGG1 (D268N contains Lys249 but is inactive, thus making the X-ray structure of the substrate bound complex available), Verdine and co-workers have made a further interesting observation concerning the position of Lys249.[21] In this case, even if the residue is close to C1, it is not placed on a trajectory suitable for an S_N2-like mechanism, and a dissociative S_N1-like mechanism cannot be a priori discarded, as suggested by recent computations carried out by Karplus and co-workers on the mono-functional uracil-DNA glycosylase (UDG).[26] Such a type of dissociative mechanism would be favored by any interaction capable of stabilizing the incipient negative charge on the oxoG during the glycosidic bond cleavage. Concerning this type of interaction, the authors observe that in the D268N structure the position of Lys249 would allow a stabilizing interaction between the cationic form of Lys249 and the oxoG π system, which should favor the base expulsion. This observation suggests the interesting hypothesis that Lys249 could be deprotonated by the forming oxoG anion.

In a subsequent paper, Karplus and co-workers[20] have examined the trapping complex that is obtained in the presence of the borohydride ion. This complex presumably originates through the reduction of the transient Schiff base intermediate that forms before starting the β-lyase reaction steps (see Scheme 2). The observed electron density for Lys249 merges continuously with that of the opened ribose fragment and is consistent with the presence of a C1-Nϵ covalent bond. Furthermore, the electron density map clearly reveals the presence of the oxoG fragment in the hOGG1 base-recognition pocket. Thus, the oxoG moiety after cleavage of the glycosidic bond is retained in the recognition pocket as the enzyme reaction advances along the β-lyase pathway. Interestingly, the authors suggest that the expelled oxoG, by deprotonating the carbon atom adjacent to the anomeric carbon, can act as an enzyme cofactor for hOGG1 for the subsequent β-lyase cascade.

As can be readily seen, a whole spectrum of mechanistic hypothesis for the catalytic activity of hOGG1 is still on the ground and under discussion. Theoretical investigations have not helped in clarifying this issue yet. In particular, as far as we know, in the literature, there is a lack of theoretical investigations on the mechanism of hOGG1. Only very recently two theoretical papers have appeared where the base excision step has been examined at the DFT level, suggesting two different mechanisms: an S_N2[27] and an S_N1[28] process. Anyway, in both cases, the used models are rather small and, most importantly, they almost completely lack of the interactions and possible steric constraints with the protein binding pocket, which may lead to crucially important effects in tuning and controlling the outcome of the process. Under this respect, it is not surprising, therefore, that Osakabe and co-workers[27] and Laaksonen and co-workers[28] find two different contrasting mechanisms.

Herein, we carry out a theoretical investigation at the DFT level of the hOGG1 glycosylase catalytic mechanism, and we try to answer some of the still open mechanistic questions. In particular, the following aspects are discussed in detail: (i) Does the base excision proceed via an S_N1-like or an S_N2-like mechanism? (ii) How can the cationic form of Lys249 be activated before undergoing the nucleophilic attack? (iii) What is the role of the Asp268 residue? To try to elucidate all of these points, we use a model system that, to the best of our knowledge, is the largest quantum mechanical model used to date. In addition, to a complete oxoG molecule and the deoxyribose ring bonded to the phosphate groups, it includes many surrounding residues that simulate the protein binding pocket and, in our opinion, can significantly affect the catalytic mechanism.

2. Choice of the Model and Computational Approach

The model system used here to emulate the hOGG1 active site (see Figure 1) has been assembled using the high-resolution crystallographic structure of a mutant hOGG1 where a Gln residue replaces Lys249. This structure is available in the Protein Data Bank with PDB code = 1EBM and resolution = 2.1 Å.[2]

This model system includes (i) the oxoG base linked to the deoxyribose ring with the two phosphate groups in position 3′ and 5′, (ii) the important fragments of the protein residues that are responsible for the recognition process of the oxidized base, (These residues are Gly42, Gln315, and Phe319.) (iii) the two water molecules W1 and W62, (iv) the Asp268 residue, (v) the Asn151, Ile152, and His270 groups that interact with the 5′ phosphate group and are responsible for significant electrostatic contributions,[29] (vi) the terminal portion of the α helix involved in the "capping" interaction (Val269-His270-Met271 residues), and (vii) the Lys249 residue. The position of the lysine residue has been obtained from the crystal structure of a wild hOGG1 bonded to an inhibitor (a DNA containing the abasic tetrahydrofuranyl THF moiety, PDB code = 1FN7, resolution = 2.6 Å).[19] This structure has been superimposed to 1EBM and then the position of the $-(CH_2)_4NH_3(+)$ group has been optimized using the same DFT level and the same model system chosen for the subsequent mechanistic investigations (see below). During this optimization process, all of the remaining atoms of the model have been kept frozen. To reduce the size of the model system, we have kept for the various residues only the portions that participate to the reaction or play a key role in the recognition process or are involved in important hydrogen bonds. Thus, for Gln315, we have considered the terminal amidic part of the residue; for Phe319, only a simple benzene ring has been included in the model, and Gly42 has been emulated by a formaldehyde molecule. Concerning the DNA strand, we have considered the p^0 and p^{-1} phosphate groups. For p^0 and p^{-1}, we have cut the C5−C4 and O3−C3 bonds, respectively, and we have replaced C4 and C3 with a hydrogen atom. The peptide bond of the Asn151-Ile152 sequence has been explicitly considered, but a methyl and ethyl group has been used to replace the α carbons of the Asn and Ile residues, respectively.

Since in our model we have eliminated a phosphate ligand interacting with the calcium ion evidenced in the crystallographic structure, to preserve the net charge of the system, we have replaced Ca(2+) with a sodium ion Na(+). The positions of this monovalent cation and its hydratation waters have been kept frozen at the initial optimized geometry (i.e., the starting

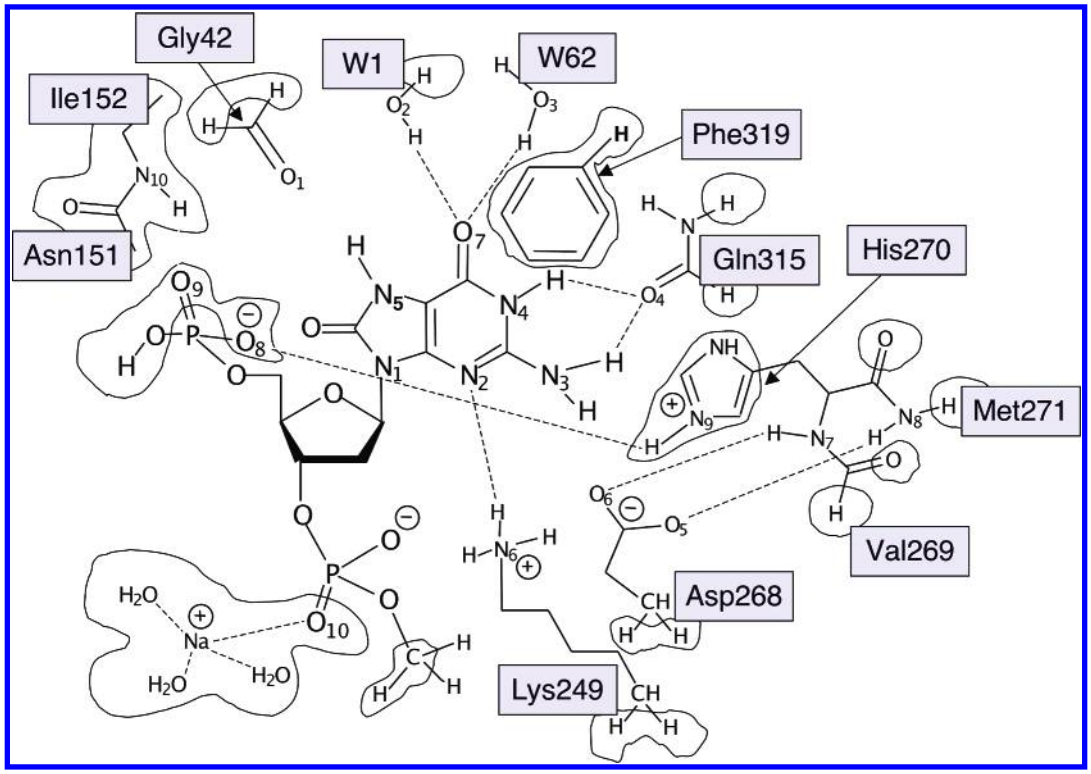

Figure 1. Schematic representation of the model system used in this paper. Atoms anchored to their crystallographic positions have been marked by contour lines.

reactant **Rx**) along the computed reaction channels. In the case of the Lys249 chain $(CH_2)_4NH_3(+)$, the α carbon has been represented by a methyl group, while Asp268 has been emulated by a propanoate fragment. Finally, the Val269 and Met271 α carbons of the terminal portion of the α-helix backbone Val269-His270-Met271 have been substituted by two hydrogen atoms. In this way, the His270 and Met271 amide N−H bonds involved in the "capping" hydrogen interactions (see Scheme 3) have been explicitly considered in our computations. An important point concerning the representation of the model system in Figure 1 should be stressed. Since in this figure we have used a two-dimensional picture, several interatomic distances are not realistic and appear much longer than in the real protein.

To preserve the geometry of the active-site cavity and thus emulate the partially constraining effect of the protein environment, during the geometry optimization procedure used to locate the critical points along the reaction pathway, we have fixed the positions of the atoms not directly involved in the reaction. These atoms have been anchored to their crystallographic coordinates as indicated in Figure 1 where they are marked by contour lines. In our opinion, this point is particularly important. We believe that the weakness of many theoretical investigations on enzyme mechanisms is represented by the unconstrained geometry optimizations applied to the molecular systems that emulate the enzyme active site. This approach, which is correct in the study of the ordinary organic reactions, introduces additional degrees of freedom in a biosystem simulation that are not truly present in the real enzyme and provides a misleading picture of many interactions.

To check the reliability of this approximation (fixing atomic coordinates at the crystallographic values), we have compared the structure used to build our model[2] to the structure of the intermediate Schiff base obtained after reduction with $NaBH_4$[20]. The overlapping of the two structures shows that the variation of the positions of the atoms that have been kept fixed in our model is actually negligible. This evidence justifies, for instance, the "freezing" of the Phe319 benzene ring.

All of the reported DFT computations have been carried out with the Gaussian 98 and 03 series of programs using the B3LYP[31] functional (which has been demonstrated to provide a reliable description of organic systems involving hydrogen bond interactions)[32,33] and locally dense basis sets (LDBS).[34] According to this approach, the system has been partitioned into different regions, which were assigned basis sets of different accuracy. One region contains the atoms directly involved in the reaction or in the formation of the most important hydrogen bonds. We have used in this case the DZVP basis, which is a local spin density (LSD)-optimized basis set of double-ζ quality.[35] This basis, which includes polarization functions, is suitable to describe weak hydrogen interactions such as those occurring in the system investigated here. For the other atoms, we have employed the smaller 3-21G and STO-3G basis sets.[30] The level of accuracy used in the description of the various atoms is described in details in Figure S1 of Supporting Information. The transition vector of the various transition states has been analyzed by means of frequency computations.

To evaluate the electrostatic effect of the protein environment on the rate-determining step of the investigated process, single-point computations were performed on the DFT optimized structures using the solvent continuous model approach (CPCM).[36−37] The ONIOM approach[38,39] as implemented in Gaussian 03 was also tentatively used, but it's result was inappropriate for this purpose. More details on the CPCM and ONIOM approaches are given in Supporting Information.

3. Results and Discussion

3.1. Potential Energy Surface. In this section, we examine in detail the singlet ground state potential energy surface (PES) obtained for the first glycosidic step and Schiff base formation on the model system shown in Figure 1. This is the catalytic

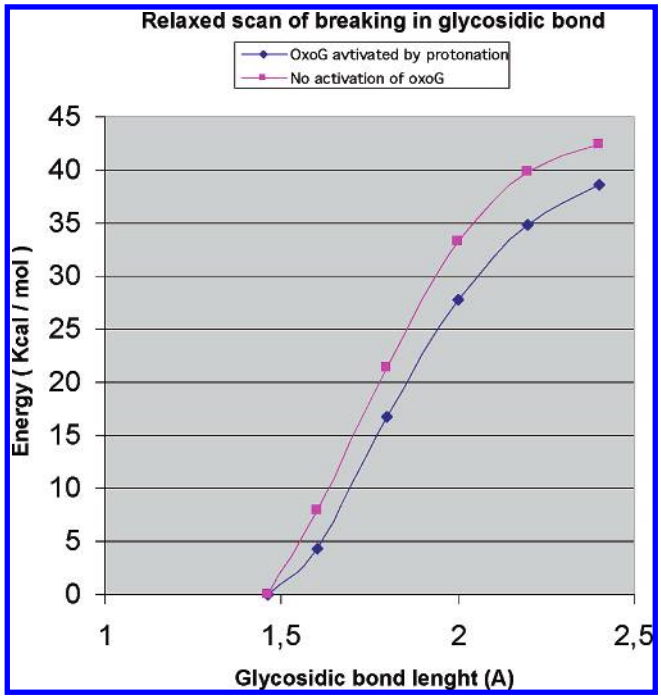

Figure 2. Relaxed scan along the glycosidic bond breaking coordinate for a hypothetical S_N1 process: the glycosidic bond is gradually stretched from 1.5 Å to 2.45 Å, and all of the remaining coordinates are optimized. Energy profiles for the activated (i.e., N2 protonated, blue line) and inactive (purple line) oxoG leaving group are shown. Note that both paths involve a much larger barrier (>35 kcal mol^{-1}) than that computed for the asynchronous S_N2 process (17 kcal mol^{-1}).

step unveiling the activity of hOGG1 in vivo, since the following lyase action (i.e., DNA backbone breaking) is performed in vivo by another enzyme, that is, APE.[24,40,41] Following the mechanistic hypothesis suggested for UDG in ref 26, an S_N1 mechanism was initially searched for, trying to locate the carbocationic intermediate following the oxoG base excision. Despite a very careful analysis performed on the PES, we could not locate this critical point, leading to the conclusion that the S_N1 path is not allowed in our model. A further check to definitely exclude the S_N1 mechanism was done by carrying out a relaxed scan along the glycosidic bond breaking coordinate corresponding to a hypothetical S_N1 process. Again, no transition state was detected (see Figure 2).

Consequently, the alternative S_N2 pathway was investigated, and the mechanism of Lys249 activation (i.e., deprotonation) was initially explored. As previously discussed, the mutagenic study has already excluded the possibility that Asp268 can act as acceptor for the Lys249 proton.[21] As a matter of fact, also the neighboring Cys253 residue could represent in principle another potential deprotonating agent for Lys249. Nevertheless, in our study, this residue was considered as already protonated and was not included in the model system, thus excluding its action in lysine activation. This decision was based on the available crystallographic structure of Lys249Gln mutants.[2] In these mutated forms, where the Gln249/Cys253 structural motif is maintained, the cysteine sulfur is closer (3.8 Å distance) to the glutamine carbonyl group than to the glutamine ammine group. This evidence suggests the existence of a protonated (and neutral) Cys253 residue forming a hydrogen bond with the glutamine carbonyl oxygen (S—H···O═C). If Cys253 were not protonated (and thus charged), the negative sulfur would be expected to form a hydrogen bond with the glutamine ammine group. This would require a rotation around the glutamine single bonds, leading to a structure significantly different from that observed. There is another aspect, which is worth it to outline. In the available D268N mutated structure for the protein—substrate complex (the only one where Lys249 is preserved), the distance between the cysteine sulfur and the lysine ammine group is compatible with the existence of a hydrogen bond. However, this does not necessarily imply a deprotonated cysteine, because a protonated Cys253 residue could equally form a hydrogen bond with lysine (N—H···S—H) using the sulfur lone pair. Finally, it is worth remembering that our hypothesis agrees with the common assumption that considers cysteine as protonated at physiological conditions.

The N2 nitrogen (see Figure 1) was finally selected as the acceptor for the Lys249 proton, following the suggestions by Goddard III and co-workers.[42] According to the calculations carried out by these authors, the N2 nitrogen is the most basic site of the oxoG base. After this proton transfer, Lys249 is activated for the S_N2 attack on the anomeric carbon while, concurrently, a more effective leaving group is created which better accommodates the increased electron density developing on the oxoG during the glycosidic bond cleavage. This activation effect is well-known in the hydrolysis of adenosine and guanosine that show an apparent first-order dependence on proton concentration over the entire (−3 to 9) pH range, reflecting the requirement for rapid protonation equilibrium of the endocyclic nitrogens of these purine bases before bond cleavage.[12,43]

The energy profile corresponding to the computed reaction path is reported in Figure 3. A schematic two-dimensional representation of the geometry of the various critical points located along it is given in Figures 4, 5, 7, and 8. For each critical point, we have reported only the most important groups of the model system and the values of the most significant geometrical parameters. The general reaction scheme that springs from the set of the computed critical points is shown in Figure 3 by the sequence I → II → III → IV → V.

A. Activation of Lys249. The initial complex **Rx** that forms upon insertion of the DNA strand (carrying the oxoG base) into the enzyme active site is schematically represented in Figure 4. A complete and more detailed three-dimensional representation of **Rx** is given in Supporting Information (Figure 2S). A complex network of hydrogen bonds characterizes **Rx**. Even if a full detailed description and analysis of all H bonds involved in this complex network is provided in Supporting Information, we would like to focus our attention on the following H bond interactions: one of the protons of Lys249 forms a rather strong H bond with the N2 nitrogen of the oxidized basis. This N6—H···N2 interaction is featured by a short H···N2 distance (1.649 Å) and prepares the proton transfer from N6 to N2, as evidenced in the reaction scheme of Figure 4. Five additional hydrogen bonds involve the two residues Gly42 and Gln315 and the water molecules (W1 and W62) of the recognition site and the oxidized basis, strongly anchoring the oxoG to the recognition binding pocket (this property will be conserved throughout the reactive process). The stabilizing capping interactions involving the Asp residue are also evident. They correspond to the rather strong O6—H···N7 and O5—H···N8 hydrogen bonds.

The first step of the process (step I: **Rx** → **ts1** → **int1**) corresponds to the proton transfer from N6 to N2 and leads both to lysine activation and to a better leaving group. In the transition state **ts1**, which is characterized by a low activation barrier (only 1.5 kcal mol^{-1}), the proton is approximately half way between N6 and N2, the H—N6 and H—N2 distances being 1.274 and 1.323 Å, respectively. The resulting intermediate **int1** is 2.7 kcal mol^{-1} lower than **Rx**. Here, the network of hydrogen

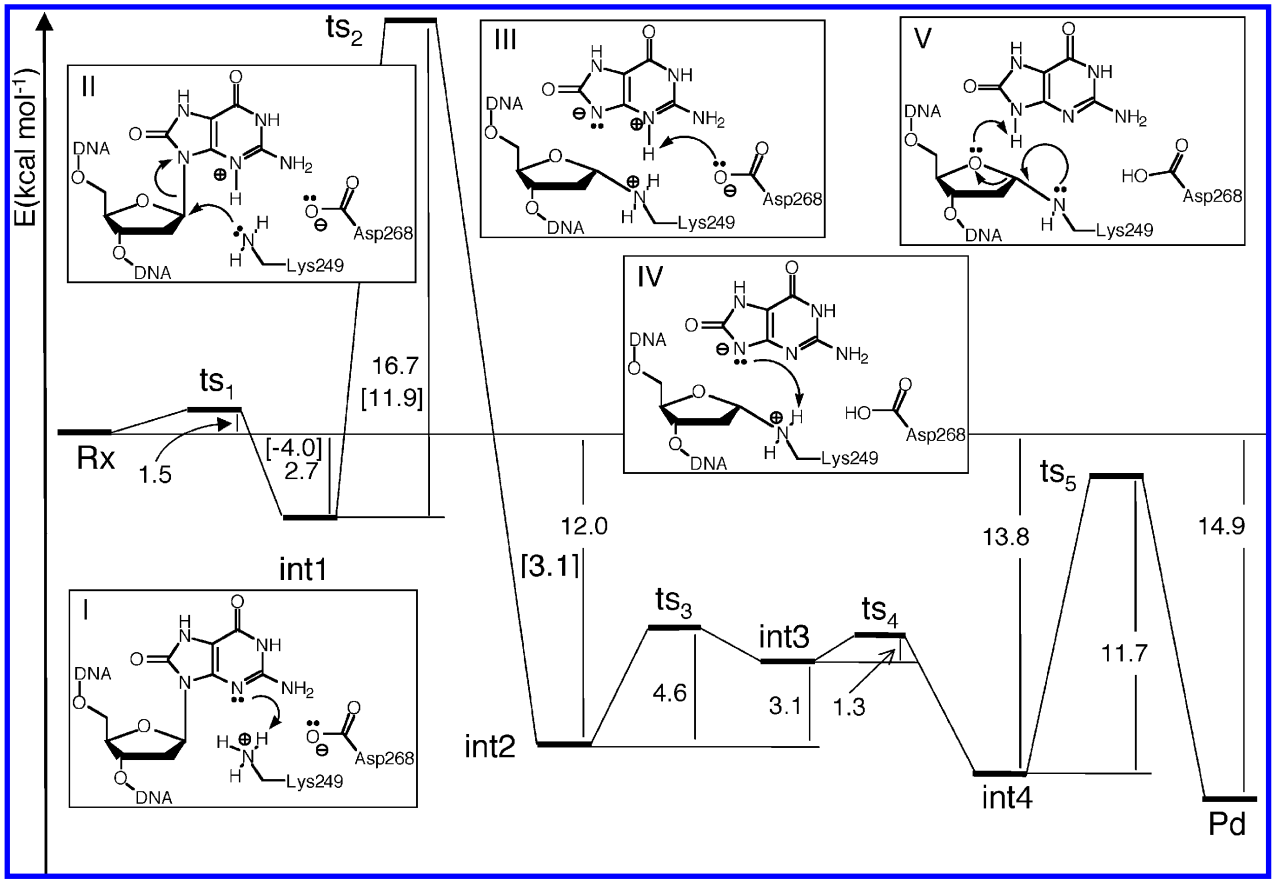

Figure 3. Energy profile obtained along the investigated reaction paths. Values in square brackets correspond to single-point CPCM computations.

bonds and the orientation of the two residues Asp268 and Lys249 do not change significantly with respect to the starting complex, with Asp268 being still involved in the "capping" interactions with the final helix groups. Interestingly, the oxoG protonation determines a slight weakening of the glycosidic bond, the C1−N1 distance increasing from 1.453 Å in **Rx** to 1.462 Å in **int1**.

B. Nucleophilic Attack and the Base Expulsion. The Lys249 deprotonation by the N2 (oxoG) atom certainly leads to the formation of a better leaving group. Under these conditions, the S_N1 process (which was previously shown to be forbidden) could become feasible. Thus, we searched again for an S_N1 mechanism. However, although activated oxoG is slightly favored with respect to the unprotonated-oxoG case, the S_N1 path is still energetically impracticable and no stable carbocationic intermediate could be detected (see Figure 2). In conclusion, our model indicates the S_N1 mechanism as highly unfavored whatever the leaving group protonation state is and points to S_N2 as the preferred pathway for the glycosidic bond breaking.

In fact, the subsequent step (step II: **int1** → **ts2** → **int2**) is the nucleophilic S_N2 attack of Lys249 on the C1 anomeric carbon. This causes the breaking of the glycosidic bond and the expulsion of the basis. This is also the rate-determining step of the process, the corresponding intrinsic activation barrier being 16.7 kcal mol^{-1} (**ts2** is 14.0 kcal mol^{-1} higher than the asymptotic limit **Rx**). Interestingly, analysis of the geometry of the transition state (see Figure 5) reveals a highly asynchronous S_N2 process: the new forming N6−C1 bond is almost completed (1.601 Å), while the glycosidic C1···N1 bond is almost fully broken (2.989 Å) at **ts2**.

To improve the description of this step (the bottleneck of the entire process), we performed a bi-dimensional relaxed scan along the two most important bonding coordinates unveiling the nucleophilic attack, that is, the C1···N1 distance (breaking glycosidic bond) and the C1···N6 distance (new forming bond, see diagram in Figure 6). At the starting point of the diagram, Lys249 has already moved from its original position in **int1**. Here, the N6···H−N2 hydrogen bond is broken, and the NH_2 group has been reoriented with the N6 lone-pair now pointing toward the C1 anomeric carbon (the C1···N6 distance is 2.75 Å, i.e. much shorter than that in **int1)**. For this new arrangement of Lys249, the glycosidic bond is weakened, and the leaving group expulsion becomes an energetically feasible process. Indeed, the surface scan depicted in Figure 6 initially displays an extended energy plateau along which the N1−C1 bond becomes almost fully broken (approximately 2.60 Å), and the energy only slightly increases (less than 8 kcal mol^{-1}). Anyway, at this stage, the nucleophile is only slightly closer to the anomeric carbon (C1−N6 distance about 2.15 Å), clearly indicating a highly asynchronous S_N2 process. Thus, reorientation of the Lys249 nucleophile from its original position in **int1** to the optimum geometric arrangement for an S_N2 attack (i.e., the initial geometry along the valley found in the bi-dimensional scan of Figure 6) and its approaching (although limited) to the anomeric carbon are essential conditions to trigger the glycosidic bond breaking process that, otherwise, would be highly unfavored, (as demonstrated by the scan of Figure 2). After this initial stage, the energy rapidly increases along the relaxed scan valley for values of the C1−N6 distance shorter than 2.15 Å. The inversion of the anomeric hydrogen and its steric interaction with the leaving oxoG base are mainly responsible for this energy increase. This interaction contributes to push further away the basis that moves up to 3 Å from C1. At this point, the formation of the N6−C1 bond can be easily completed.

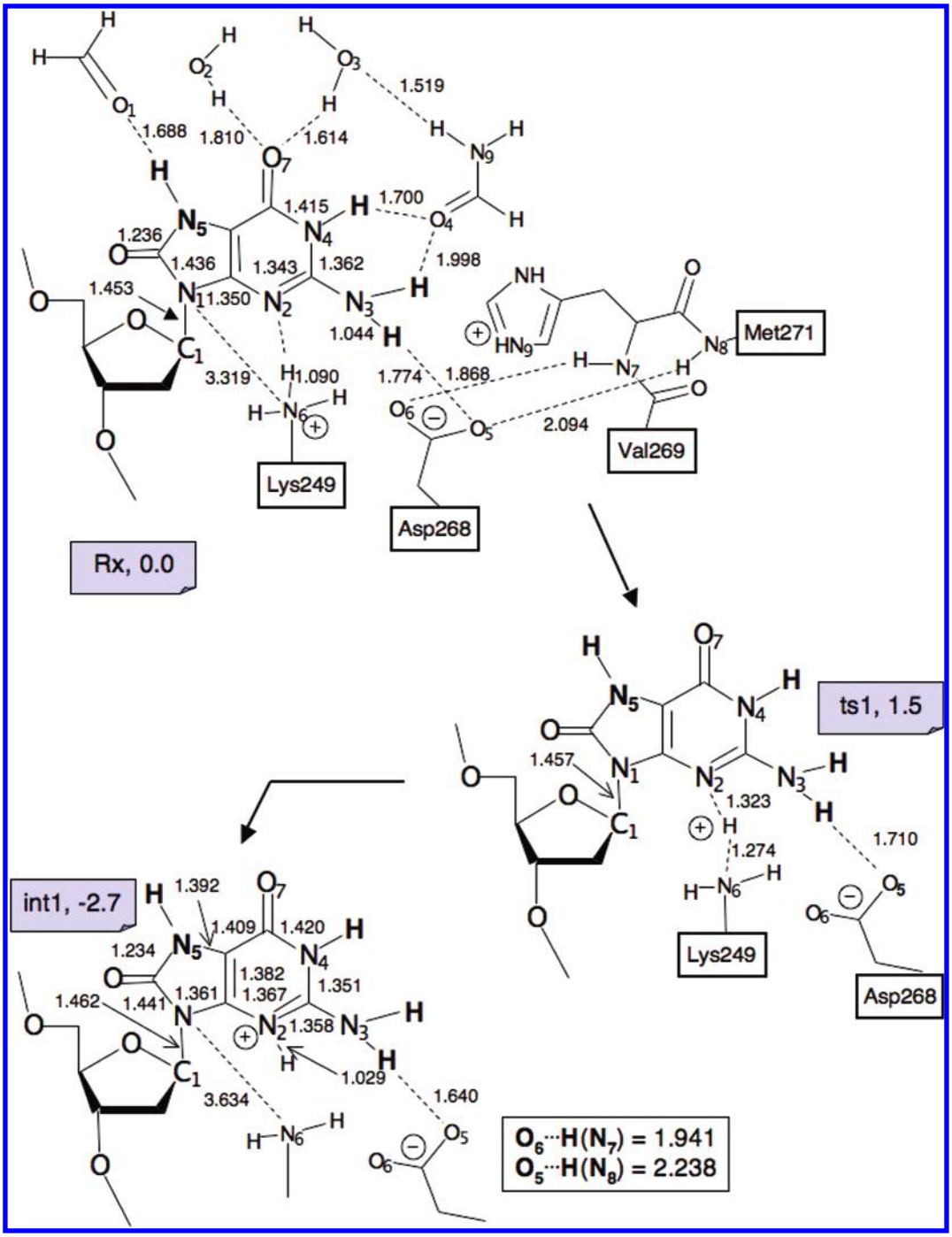

Figure 4. Schematic representation of the structure of the critical points Rx, ts1, and int1 (bond lengths are in Å, and angles are in degrees). The energy values (kcal mol^{-1}) are relative to Rx.

In conclusion, the picture that stems from the diagram of Figure 6 nicely accounts for the origin of the highly asynchronous S_N2 process recognized in step II. As a matter of fact, this process retains some features of the S_N1 mechanism. In particular, at the beginning of the reaction (i.e., along the flat energy valley), a transient carbocationic-like species is formed. The structure of this species is rather similar to that expected for a carbocationic S_N1 intermediate, but it never corresponds to a real critical point of the surface.

Perhaps, the most interesting structural feature of **ts2** is the new orientation of the capping (Asp268) residue: this has rotated with respect to its original position found in **Rx** and **int1** causing significant changes in the "capping" interactions. In the new position, one oxygen atom of the aspartate carboxylate group (O6) forms two H bonds with the two N−H groups of the Val269−His270−Met271 sequence. These H bonds are N7−H···O6 (H···O6 = 2.010 Å) and N8−H···O6 (H···O6 = 2.085 Å). The other aspartate oxygen (O5) still interacts with the oxoG amino group by the N3−H···O5 H bond (H···O5 distance = 1.953 Å) but is now involved in an additional rather strong H bond with the N2−H group of the oxidized basis (H···O5 distance = 1.664 Å, see Figure 5). Thus, the new position of the Asp268 residue has the effect of replacing the O5···H(N8) "capping" interaction with the O6···H(N8) interaction and has the advantage of introducing the new strong O5···H(N2) hydrogen bond. This new structural arrangement certainly contributes to stabilize **ts2** and lower the barrier. It is interesting to outline that the new orientation of the Asp268 residue is in agreement with the position of this residue found in a very recent crystallographic study (structure PDB code = 1YQK).[44] Another

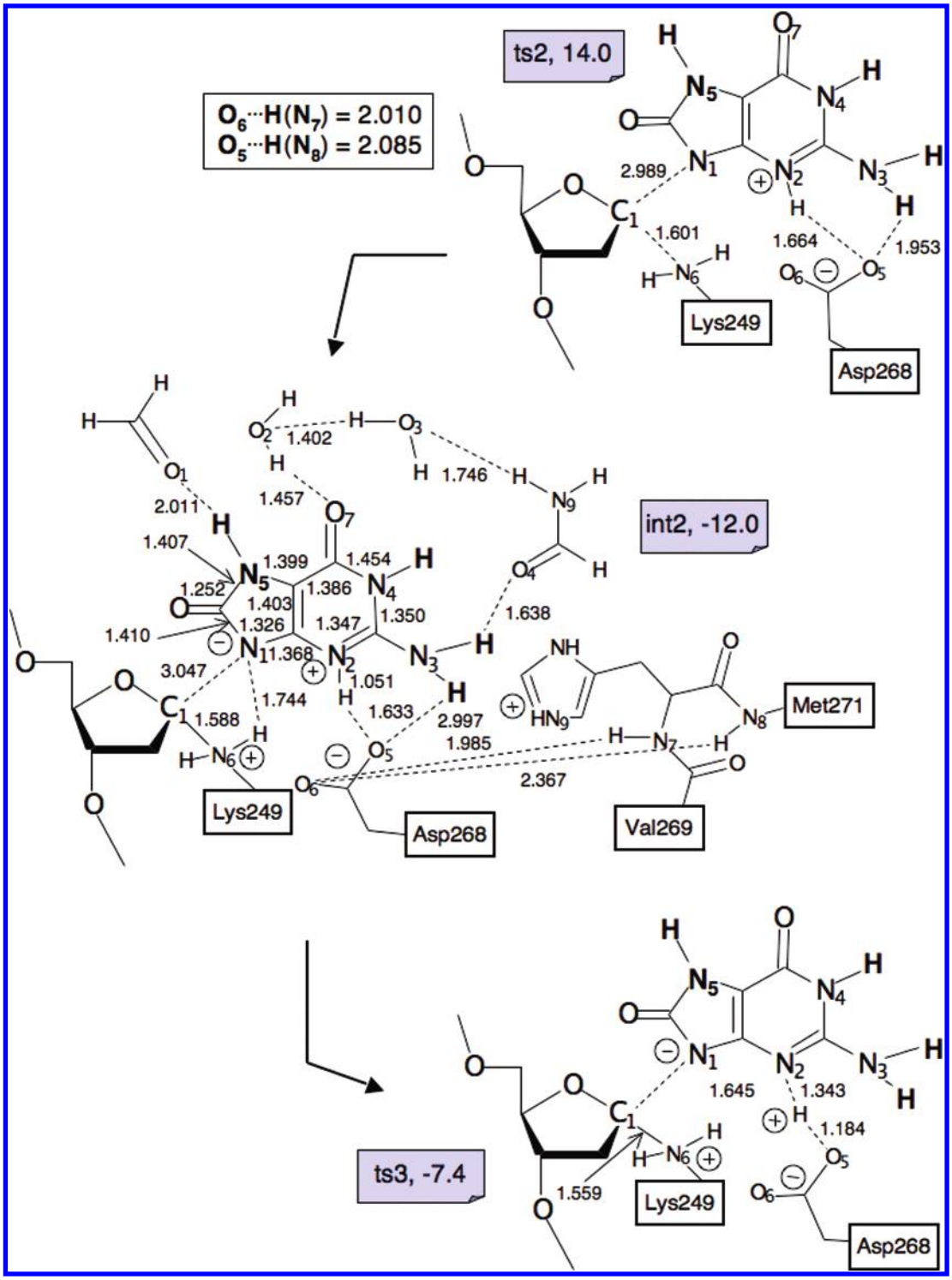

Figure 5. Schematic representation of the structure of the critical points ts2, int2, and ts3 (bond lengths are in Å, and angles are in degrees). The energy values (kcal mol^{-1}) are relative to Rx.

contribution to the **ts2** stabilization is given by the conformational arrangement of the deoxynucleoside sugar that is planar in **ts2** and, thus, maximizes the resonance stabilization of the transient oxocarbenium state during the cleavage of the glycosidic bond.[12]

In the resulting new intermediate **int2** (12.0 kcal mol^{-1} more stable than **Rx**), the expelled basis is neutral but has two opposite formal charges on N1 (negative) and N2 (positive). This new charge distribution determines significant structural changes in the five-member oxoG ring with respect to **int1** as shown in Figures 3 and 4. These geometrical variations can be easily understood on the basis of simple resonance structures involving the N1 lone pair. In **int2**, the deoxynucleoside sugar has recovered its natural 'envelope' conformation. Also, the C1−N1 distance has become 3.047 Å, but the expelled basis is still anchored to the protein residues by strong hydrogen bonds (N5−H···O1, O2−H···07, N3−H···O4, see Figure 4). The Asp268 residue in its new orientation maintains the "capping" interactions found in **ts2**, that is, the N7−H···06 and N8−H···06 hydrogen bonds, although they are slightly weaker than in **Rx** and **int1**. The other oxygen (O5) has almost lost the N3−H···O5 interaction, but the N2−H···O5 hydrogen bond has become

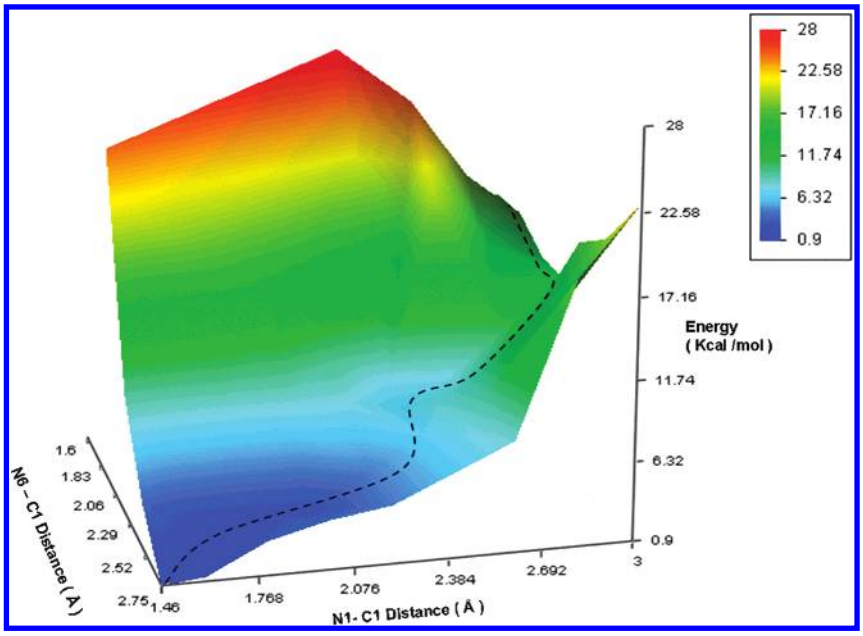

Figure 6. Bidimensional relaxed scan along the breaking C1−N1 glycosidic bond and the forming C1−N6 bond for the S_N2 process. The glycosidic bond is gradually stretched (from 1.46 to 3.00 Å) and the Lys249 is brought closer to the C1 carbon (from 2.75 to 1.6 Å) using 0.2 Å steps. All of the remaining coordinates are freely optimized.

stronger, as indicated by the H···O5 distance, which is 1.633 Å. This H bond anticipates the N2 → O5 proton transfer occurring in the following step (step III: **int2** → **ts3** → **int3**).

The N2 → O5 proton transfer requires the overcoming of a barrier of 4.6 kcal mol^{-1}. In **ts3** (see Figure 5), the proton is almost completely transferred to O5, the H···O5 and H···N2 distances being 1.184 and 1.343 Å, respectively. This proton transfer affords a new intermediate **int3** (see Figure 7), which is 3.1 kcal mol^{-1} less stable than **int2**. It is interesting to note that, while all of the H bonds that anchor the expelled basis to the protein remain almost identical on passing from **int2** to **int3**, the "capping" interactions become weaker, with the two H··· O6 distances now being 2.209 and 3.040 Å (as expected since Asp268 has become neutral).

A second proton transfer (step IV: **int3** → **ts4** → **int4**) from the N6 positive nitrogen (the original lysine nitrogen now bonded to C1) to the negative oxoG nitrogen N1 leads to **int4** (see Figure 7) by overcoming a very low barrier (only 1.3 kcal mol^{-1}) and completes the base structural rearrangement. Thus, the double proton transfer (steps III and IV), where the Asp268 residue plays a key role, has the effect of moving one proton from N2 to N1, a key position to complete the process in the final step (Schiff base formation, see below). The resulting intermediate after the double proton transfer **int4** is 4.9 kcal mol^{-1} lower than **int3** and 13.8 kcal mol^{-1} more stable than the initial complex **Rx**.

C. Formation of the Schiff Base Product. The final step (step V: **int4** → **ts5** → **Pd**) is a concerted process where a proton moves from the base nitrogen atom N1 to the ribose ring oxygen causing the simultaneous breaking of the ring C1−O bond and the forming of a double C1−N6 bond. All of these simultaneous transformations are evident in the transition state **ts5** (see Figure 8). Here, the proton is approximately half way between N1 and the ring oxygen, the H−N1 and H−O distances being 1.200 and 1.282 Å, respectively. The C1−O bond is 2.294 Å, and a significant shortening of the C1−N6 bond is observed (from 1.496 Å in **int4** to 1.315 Å in **ts5**). The activation barrier required for this final transformation is 11.7 kcal mol^{-1}. In Figure 8, a schematic representation of the protonated Schiff base product (**Pd**) is given. In **Pd**, which is 14.9 kcal mol^{-1} more stable than the starting complex **Rx**, the oxoG base has a negative charge formally localized on N1, while the nitrogen atom N6 is now positively charged. The rupture of the C1−O bond is completed (C1−O distance = 3.018 Å) while the C1−N6 bond is definitely a double bond (C1−N6 distance = 1.293 Å). Finally, the position of the expelled base within the active site does not significantly change. It remains anchored to the active site residues through a complex network of hydrogen bonds as observed in **int2** and **int3**.

3.2. Computational Background. It is worth comparing previous theoretical models with the current one. As a matter of fact, there is a general lack of computational information on this problem and, to the best of our knowledge, only two theoretical papers[27,28] have recently appeared on this topic. In the first paper, Osakabe and co-workers[27] have carried out B3LYP/6-31G(d,p) computations on a small model system formed by Lys249 (emulated by protonated methyl amine), the ribose ring, and the five-membered ring of 8-oxoG. They found that the cleavage of the base involves three elementary reaction steps. In particular, the first step corresponds to the activation of the protonated lysine (a proton is removed from the Lys249 ammonium group by the oxoG carbonyl group) that can undergo a nucleophilic (S_N2) attack on the ribose C1 carbon in the subsequent step. In the second paper, Laaksonen and co-workers found evidence for an S_N1 type mechanism.[28] These authors propose a mechanism (that corresponds to the smallest energy barrier) where the cationic lysine residue electrostatically stabilizes the dissociating anionic oxoG. Then, the lysine transfers a proton to the expelled base to further stabilize it. This hypothesis agrees with that of Verdine and co-workers based on the D268N crystallographic structure (see discussion in the introduction section).[21] The formation of a Schiff base completes the process.

In our opinion, these results are rather questionable. The most valuable objection is that in both papers the authors use rather small models, where the interactions and the possible steric constraints due to the protein binding pocket are almost completely lacking. These interactions can be certainly crucial in determining the catalytic activity. In particular, the first proposed mechanism[27] requires a conformational rearrangement

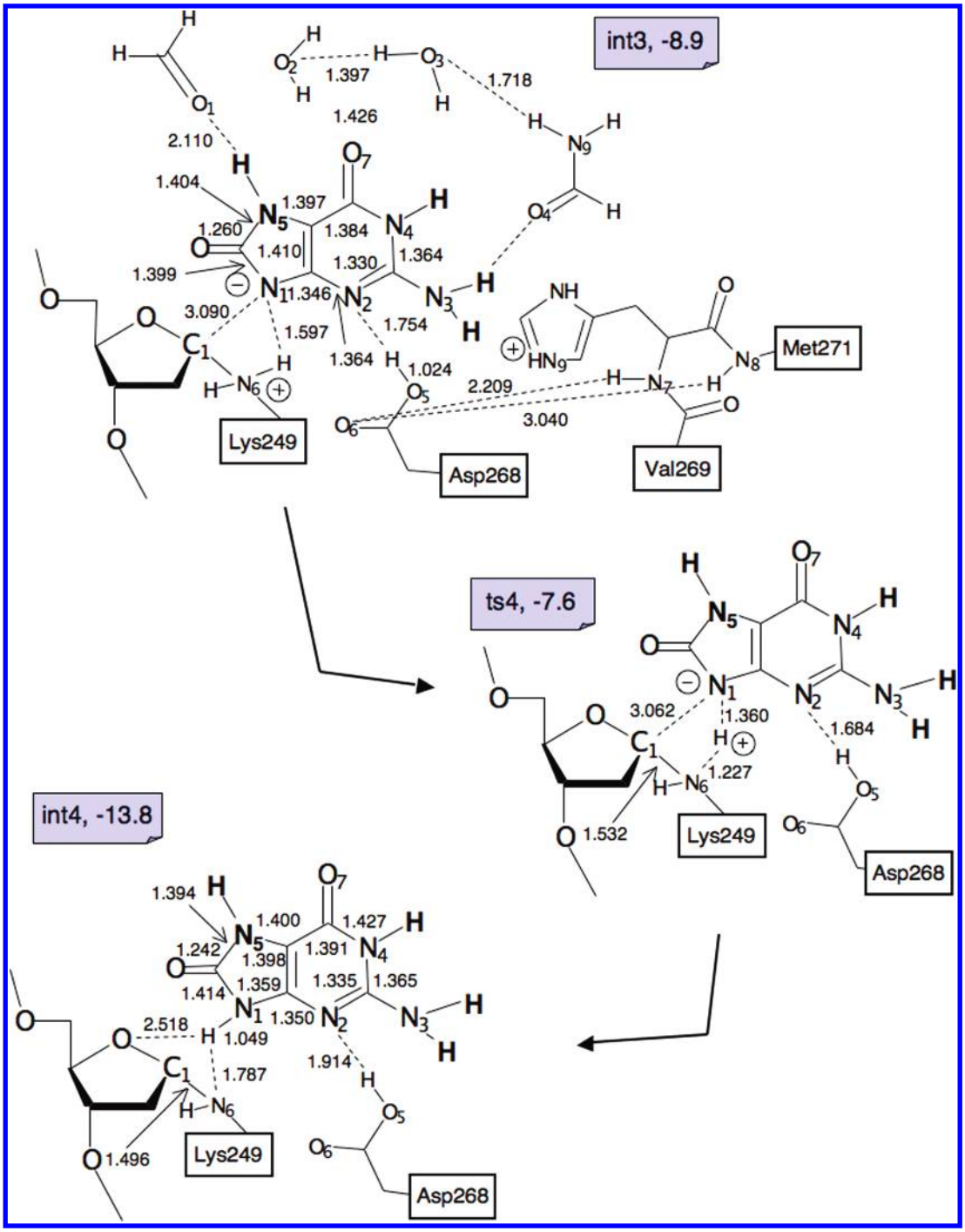

Figure 7. Schematic representation of the structure of the critical points int3, ts4, and int4 (bond lengths are in Å, and angles are in degrees). The energy values (kcal mol^{-1}) are relative to Rx.

of the oxidized basis that is possible only within a small model system but becomes rather unlike the real enzyme where the oxidized basis is strongly anchored to several residues which are omitted if the model is too small. Similarly, the small size of the model can seriously affect the evidence for the second mechanism,[28] as the authors themselves outline. Therefore, it is not surprising that these two works lead to different and opposite mechanistic hypothesis (S_N2 vs S_N1). We would like to stress once again that the model used in the present work takes into account for the first time some important effects due to steric constraints and electrostatic interactions of nearby residues that are involved in tuning and controlling the outcome of the process. Although other possible important contributions have been ignored (for instance the effect of neglecting the protein−solvent environment), we would like to stress that here we are modeling the problem at an unprecedented level of accuracy for a QM system. The model system is much larger than that used in other similar studies (it includes all atoms in an 8 Å radius from the reactive center), and we believe that a reliable mechanistic picture may be drawn.

3.3. Leaving Group Activation. Activation of the leaving group seems to be a recurring catalytic strategy in both solution and enzymatic cleavage of the glycosidic bond in the purine nucleoside. We have just discussed the apparent first-order dependence on proton concentration of the solution hydrolysis of the purine nucleoside, indicating that the protonated nucleoside is the reactive species.[43] Several enzymatic cleavages have been suggested to proceed via an analogous mechanism involv-

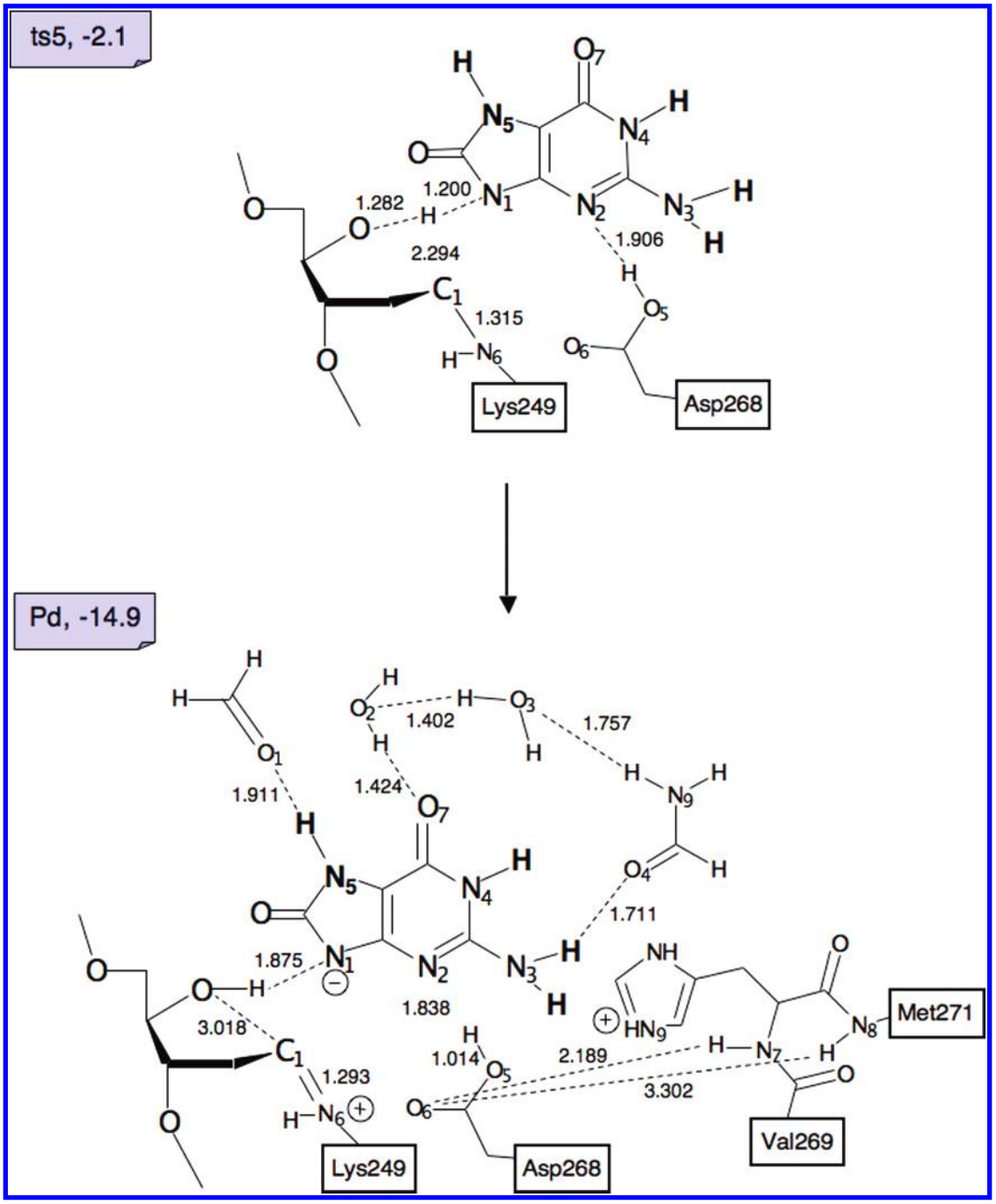

Figure 8. Schematic representation of the structure of the critical points ts5 and Pd (bond lengths are in Å, and angles are in degrees). The energy values (kcal mol^{-1}) are relative to Rx.

ing pre-equilibrium protonation of the substrate by an acidic group of the enzyme.[45−50] Our model suggests a similar behavior for hOGG1. However, in this case, the nucleophilic group itself (LYS 249) protonates the most basic site of the oxoG base[42] (nitrogen number 2 in Figure 4) and triggers the catalytic mechanism. This could be a further control, preparing base excision, which has the advantage of activating both the leaving group and the nucleophile in the same step.

Therefore, this work seems to enforce the hypothesis that cleavage of purine and pyrimidine bases follow different mechanisms (as highlighted by Stivers and Jiang in ref 12) because a viable proton acceptor group is absent in pyrimidine bases. Consequently, it is more correct to compare the mechanism of hOGG1 to that of the bacterial MutY enzyme[45] (a purine-repairing system) instead of to the mechanism of UDG[26] (a pyrimidine-repairing system, where in fact a dissociative S_N1-type mechanism has been suggested, see ref 26), as it is often done.

3.4. Capping Interactions and Glycosylase Activity: Experiments Versus Computations. As briefly described in the introduction, Verdine and co-workers[21] have carefully analyzed the role of the invariant Asp268 residue in hOGG1. They have considered various mutated forms of hOGG1 by replacing the Asp residue with Asn (D268N), Glu(D268E), and Gln (D268Q) and have suggested the importance of the Asp268 N-cap interaction (see Scheme 3) in stabilizing the protein folding. In agreement with this hypothesis, they have observed that the mutation of Asp268 to Glu and Gln (which cannot retain capping interaction) seriously affects the thermal stability of hOGG1 (the D268Q mutant protein is prone to denaturation during

purification). On the contrary, mutation of Asp268 to Asn (D268N), a residue capable of maintaining capping interactions, preserves the stability of the protein. However, while D268N has almost completely lost its catalytic activity, D268E and D268Q are, surprisingly, still active.

We believe that our computational results offer a better understanding of this scenario. Indeed, we have provided computational clues that the Asp268 residue does not act as a deprotonating agent for Lys269, in agreement with mutation experiments and the retained activity of the D268Q mutant. More specifically, its role in the rate-determining step of the S_N2 type mechanism (**ts2** in step II, see Figure 4) is to provide an additional stabilization of the protonated neutral oxoG leaving group (via H bond interactions) and not only of the cationic deoxyribose fragment[21] (see **int2** intermediate). Anyway, this effect must be minor since it is paid at the expense of the strong capping interactions (note that capping interactions are decreased in **int2**). Remarkably, this suggests that this stabilization effect could be even stronger if such a group would not act as an helix cap, being directly available for this purpose, as it is the case for the Glu and Gln residues in the D268E and D268Q mutants. This could represent a possible explanation for the preserved activity observed in these mutated enzymes. Moreover, it is worth noting that Asp268 is directly involved in the double proton-transfer process (steps III and IV) preparing the last reactive step (step V) leading eventually to a ribose ring opening and to a reduction of the capping interactions (**Pd**). Anyway, this is not the rate-determining step of the reaction, being far lower in energy (see Figure 2), and it is reasonable to think that a competing alternative process (although slightly less favored) may become operative in the absence of the Asp268 mediating agent, thus preserving the catalytic activity of the aforementioned mutated proteins. For example, Lys249 may be directly deprotonated by the negative N1 nitrogen atom in **int2** without the assistance of Asp268 in step III (whose effect is to increase the basicity of the oxoG fragment). Obviously, this would cost a little bit more (i.e., higher barriers), but on the other hand, the following protonation of the ribose oxygen (which triggers its opening in the final reactive step) would be facilitated. Since these steps are not rate-determining for the process, it is realistic to consider all of these mechanistic alternatives as possible (note that the catalytic activity of the D268E and D268Q mutated forms is the same as that of the wild type).

A speculation about the lost catalytic activity of the D268N mutated form may be attempted. As shown by Verdine and co-workers[18] and on the basis of the available D268N crystallographic structure, Asn preserves the capping stabilization, but the position of Lys249 (although close to C1) is not suitable for an S_N2-like mechanism. Since our computations point to an S_N2-type process (although highly asynchronous) as the rate-determining step and this attack appears to be prevented (or at least much less favored) in the specific D268N arrangement, we think this could be the reason for the observed lack of catalytic activity in this mutant. This would also suggest that a change in mechanism to a dissociative S_N1 type is not likely to occur in OGG1. Furthermore, we should point out that Asn cannot mediate the double proton-transfer process since it cannot operate as a deprotonating agent (similarly to Gln) but can operate only as a H bond acceptor. However, since Asn (unlike Gln) preserves strong capping interactions, it cannot simultaneously act as a N2−H bond acceptor. On the other hand, Gln (which is not involved in capping interactions) can form O···H−N2 hydrogen bonds, thus assisting the leaving group expulsion (i.e., the rate determining step) and the following N6−H(+) deprotonation (i.e., step IV) by increasing oxoG basicity (although it cannot directly deprotonate N2, step III, as Asp and Glu do).

Furthermore, please note that the weakening in the capping interaction upon going from **Rx** to **Pd** along the catalytic path reduces the protein folding stability, and this may help the expulsion of the reaction products (i.e., the abasic DNA fragment and the cleft oxoG base). Obviously, this would only be a temporary effect, since Asp268 can be quickly deprotonated by the water environment in a following step, restoring the original capping interactions, and the enzyme will be ready for a new catalytic cycle.

Finally and very remarkably, the value of the intrinsic activation barrier computed for the rate-determining step of the process (16.7 kcal mol^{-1}) agrees quite well with the experimental estimate[24,25,51] of 17.1 kcal mol^{-1}, leading to a further validation of the reliability of the model system and the computed mechanism.

3.5. Product (Pd) of Glycosylase Activity: Stabilization Effects. In the product complex **Pd** (14.9 kcal mol^{-1} more stable than the starting complex **Rx**), the oxoG base has a negative charge formally localized on N1, while the nitrogen atom N6 is now positively charged. Although this may appear quite surprising at a first glance, we see that the aromatic anion is heavily stabilized by several cooperative effects: (i) delocalization/resonance effects involving the negative charge on N1, (ii) H-bonds network involving both the residues of the recognizing site, Asp268, and the opened ribose ring (see **Pd** structure in Figure 6), (iii) electrostatic stabilization due to the adjacent cationic residues (His270 and the Lys249 protonated Schiff base), and (iv) π-stacking effects by the proximal Phe319 aromatic residue.

In particular, the two carbonyl groups play a key role in determining the resonance stabilization (i) of the negative oxoG base, as it is evident from the possible contributing structures describing oxoG. This is perhaps one of the strongest effects in stabilizing the expelled oxoG fragment and provides the thermodynamic driving force for the catalytic process to occur. It is worth noting that this effect should be much weaker in the native unoxidized base G (where one carbonyl group is lacking). Thus, nature exploits at its best the chemical−physical properties of the damaged system to trigger glycosylase activity.

3.6. Effects of the Electrostatic (Protein−Solvent) Environment. In the present section, we try to discuss on a qualitative ground the effect of neglecting the protein and solvent environment, and we provide a justification for this approximation involved in our model of hOGG1.

Although a solvation effect cannot be ruled out a priori and, in principle, can significantly affect the mechanistic picture, we believe that its role is minor in the present case. Concerning this point, it is important to note that, after the formation of the preliminary Michaelis complex **Rx** (binding of the substrate to the protein), the active site (including Lys249 and oxoG) is much less accessible to solvent than in free hOGG1 (unbound protein). Thus, the role of solvation should be less important than expected, and ignoring it may be a reasonable approximation. This point is central to our problem, since we suggest that Lys249 deprotonation (step I) represents a key step for the catalysis, by triggering the nucleophile and leaving group activation. Neglecting solvation effects could lead, in principle, to an unstable and unrealistic protonated lysine (i.e., a sort of computational artifact), thus biasing the discussion in favor of

the mechanism proposed here. In our opinion, this is not the case, and the analysis above-reported (concerning the structural features of the bound protein active site) should partly justify our approximation. Another important point is the following. Since both reactants (**Rx**) and products (**int1** i.e. the protonated N2−oxoG cationic system) are equally charged, solvation (provided it is important) should similarly affect the energy of the two points, and the computed reaction profile should not be significantly modified. This conclusion would be certainly weak for a neutralization process where a charged reactant leads to a neutral product (whose stabilization by solvation can be significantly lower).

To obtain a rough estimate of the electrostatic effect of solvation and protein environment (in particular, the stabilization of the starting protonated Lys249) we performed single point CPCM calculations (see section 2) on some selected mechanistically important points along the path, namely **Rx**, **int1**, **ts2**, and **int2**. The values obtained with the CPCM approach are reported in square brackets in Figure 3. As expected, these computations do not substantially modify the energy profile and the mechanistic scenario, although step I becomes slightly endo-ergonic (only by 4 kcal mol^{-1}, see below).

In particular, the energy of both **int1** and **int2** increases with respect to the asymptotic limit (they are now 4.0 and 3.1 kcal mol^{-1} above and below this reference point, respectively), but their difference (9.3 kcal mol^{-1}) does not change too much with respect to the gas-phase model (7.1 kcal mol^{-1}). More important, the transition state for the rate-determining step (**ts2**) is now 15.9 kcal mol^{-1} above the asymptotic limit. This value agrees fairly well with the corresponding value obtained in vacuo (14.0 kcal mol^{-1}). Consequently, we have solid grounds for retaining the still valuable proposed hypothesis for the leaving group activation and the glycosydic bond breaking.

4. Conclusions

In this paper, we have carried out a DFT study on the catalytic mechanism of the DNA glycosylase hOGG1. To this purpose, we have used an extended QM model system that has provided new important insights into this problem. Specifically, we have described in detail a new mechanism for the enzyme activation, the cleavage of the glycosidic bond, and the expulsion of the damaged base, which generates an enzyme−DNA adduct (a protonated Schiff base). The most significant results can be summarized as follows:

(i) The Asp268 residue does not play any role in the Lys249 activation. This residue is involved in the "capping" interactions with the amide protons of the Val269−His270−Met271 fragment (i.e., the amide groups located along the first turn following Asp268 at the N-terminal end of an α helix).

(ii) The activation of the protonated Lys249 is easily carried out by the oxidized basis oxoG that acts as a coenzyme in the catalytic cycle. The proton transfer from Lys249 to oxoG requires a very low activation barrier (only 1.5 kcal mol^{-1}) and has the effect of weakening the C1−N1 glycosidic bond.

(iii) The activation of the leaving group triggers the cleavage of the glycosidic bond, showing a recurring catalytic strategy in the enzymatic cleavage of purine nucleoside, that is, protonation of the nucleoside base by an enzymatic general acid.

(iv) The rate-determining step of the process is represented by the nucleophilic attack of Lys249 on the anomeric carbon, which determines the base expulsion. In this nucleophilic attack, the orientation of the Asp268 residue significantly changes in such a way to make possible new hydrogen bonds that contribute to stabilize the transition state and lower the activation barrier (16.7 kcal mol^{-1}). Remarkably, this is in reasonable agreement with the experimental estimate of 17.1 kcal mol^{-1}.

(v) After the expulsion, the basis remains anchored to the active site residues by means of strong hydrogen bonds. This is in agreement with the observation of Karplus and Verdine[20] that, after cleavage of the glycosidic bond, the expelled oxoG moiety is retained in the enzyme recognition pocket.

(vi) Following basis expulsion, the Asp268 residue plays a key role in a double proton-transfer process occurring in two steps. This process has the final effect of protonating the negative oxoG nitrogen N1 initially bonded to C1. Eventually, this proton activates the ribose ring opening and triggers the formation of the Schiff base product. Thus, the expelled oxoG plays again as an enzyme cofactor at the end of the process, as it does at the beginning for nuclephilic Lys249 activation.

Acknowledgment. We would like to thank M.U.R.S.T. (Cofin 2005, Progetto Nazionale "Sintesi e Stereocontrollo di Molecole Organiche per lo Sviluppo di Metodologie Innovative di Interesse Applicativo") and Bologna University (Progetti Strategici d'Ateneo 2005: Progetto CompRenDe) for the financial support of this research. M.G. is also grateful for a FIRB (RBAU01L2HT). We wish to thank CINECA and INSTM for granted calculation time.

Supporting Information Available: Undocumented computational details (S1) and results (S2), the Cartesian coordinates (S3) of all the structures discussed in the text, and related figures (Figures S1−S2). This material is available free of charge via the Internet at http://pubs.acs.org.

References and Notes

(1) Michaelis, M. L.; Miller, J. *J. Bacteriol*. **1992**, *174*, 6321−6325.
(2) Bruner, S.; Norman, D. P. G.; Verdine, G. L. *Nature* **2000**, *403*, 859−866.
(3) Elhai, A.; Zheng, Z.; Park, J.; Eyring, K.; McCaffrey, T.; Lazarus, P. *Carcinogenesis* **2002**, *23*, 1229−1234.
(4) Marnett, L. J. *Carcinogenesis* **2000**, *21*, 361−370.
(5) Boiteux, S.; Radicella, J. *Arch. Biochem. Biophys.* **2000**, *377*, 1−8.
(6) Grollman, A. P.; Moriya, M. *Trends Genet.* **1993**, *9*, 246−249.
(7) Hainout, P.; Hernandez, T.; Robinson, A.; Rodriguez-Tome, P.; Flores, T.; Hollstein, M.; Harris, C. C.; Montesano, R. *Nucleic Acids Res.* **1998**, *26*, 205−213.
(8) Scharer, O. D.; Jiricny, J. *BioEssays* **2001**, *23*, 270−281.
(9) Hollis, T.; Lau, A.; Ellenberger, T. *Prog. Nucleic Acid Res. Mol. Biol*. **2001**, *68*, 305−314.
(10) McCollough, A. K.; Dodson, M. L.; Lloyd, R. S. *Annu. Rev. Biochem.* **1999**, *68*, 255−285.
(11) Fromme, J. C.; Banerjee, A.; Verdine, G. L. *Curr. Opin. Struct. Biol.* **2004**, *14*, 43−49.
(12) Stivers, J. T.; Jiang, Y. L. *Chem. Rev.* **2003**, *103*, 2729−2759.
(13) Krokan, H. K.; Standal, R.; Slupphaug, G. *Biochem. J.* **1997,** *325*, 1−16.
(14) Nash, H. M.; Bruner, S. D.; Scharer, O. D.; Kawate, T.; Addona, T. A.; Spooner, E.; Lane, W. S.; Verdine, G. L. *Curr. Biol*. **1996**, *6*, 968−980.
(15) Labahn, J.; Scharer, O. D.; Long, A.; Ezaz-Nikpay, K.; Verdine, G. L.; Ellenberger, T. E. *Cell* **1996**, *86*, 321−329.
(16) Bjoras, M.; Seeberg, E.; Luna, L;, Pearl, L.; Barret, T. *J. Mol. Biol.* **2002**, *317*, 171−177.
(17) von Hippel, P. H.; Berg, O. H. *J. Biol. Chem.* **1989**, *264*, 675−678.
(18) Panayotou, G.; Brown, T.; Pearl, L. H.; Savva, R. *J. Biol. Chem.* **1998**, *273*, 45−50.
(19) Norman, D. P. G.; Bruner, S. D.; Verdine, G. L. *J. Am. Chem*. Soc. **2001**, *123*, 359−360.
(20) Fromme, J. C.; Bruner, S. D.; Yang, W.; Karplus, M.; Verdine, G. L. *Nat. Struct. Biol.* **2003**, *10*, 204−211.
(21) Norman, D. P. G.; Chung, S. J.; Verdine, G. L. *Biochemistry* **2003**, *42*, 1564−1572.
(22) Chung, S. J.; Verdine, G. L. *Chem. Biol.* **2004**, *11*, 1643−1649.
(23) Morland, I.; Luna, L.; Gustad, E.; Seeberg, E.; Bjoras, M. *DNA Repair* **2005**, *4*, 381−387.

(24) Vidal, A. E.; Hickson, I. D.; Boiteaux, S.; Radicella, J. P. *Nucleic Acid Res.* **2001**, *29*, 1285−1292.
(25) Hill, J. F.; Hazra, T. K.; Izumi, T.; Mitra, S. *Nucleic Acid Res.* **2001**, *29*, 430−438.
(26) Dinner, A. R.; Blackburn, G. M.; Karplus, M. *Nature* **2001**, *413*, 752−755.
(27) Osakabe, T.; Fujii, Y.; Hata, M.; Tsuda, M.; Neya, S.; Hoshino, T. *Chem.-Biol. Inf. J.* **2004**, *4*, 73−92.
(28) Schyman, P.; Danielsson, J.; Pinak, M.; Laaksonen, A. *J. Phys. Chem. A* **2005**, *109*, 1713−1719.
(29) Jiang, Y. L.; Ichikawa, Y.; Song, F.; Stivers, J. T. *Biochemistry* **2003**, *42*, 1922−1929.
(30) Frisch, M. J.; Trucks, G. W.; Schlegel, H. B.; Scuseria, G. E.; Robb, M. A.; Cheeseman, J. R.; Zakrzewski, V. G.; Montgomery, J. A., Jr.; Stratmann, R. E.; Burant, J. C.; Dapprich, S.; Millam, J. M.; Daniels, A. D.; Kudin, K. N.; Strain, M. C.; Farkas, O.; Tomasi, J.; Barone, V.; Cossi, M.; Cammi, R.; Mennucci, B.; Pomelli, C.; Adamo, C.; Clifford, S.; Ochterski, J.; Petersson, G. A.; Ayala, P. Y.; Cui, Q.; Morokuma, K.; Malick, D. K.; Rabuck, A. D.; Raghavachari, K.; Foresman, J. B.; Cioslowski, J.; Ortiz, J. V.; Stefanov, B. B.; Liu, G.; Liashenko, A.; Piskorz, P.; Komaromi, I.; Gomperts, R.; Martin, R. L.; Fox, D. J.; Keith, T.; Al-Laham, M. A.; Peng, C. Y.; Nanayakkara, A.; Gonzalez, C.; Challacombe, M.; Gill, P. M. W.; Johnson, B. G.; Chen, W.; Wong, M. W.; Andres, J. L.; Head-Gordon, M.; Replogle, E. S.; Pople, J. A. *Gaussian 98*, revision A.6; Gaussian, Inc.: Pittsburgh, PA, 1998.
(31) Becke, A. D. *J. Chem. Phys.* **1993**, *98*, 5648−5652.
(32) (a) Ziegler, T. *Chem. Rev.* **1991**, *91*, 651−667. (b) Fan, L.; Ziegler, T. *J. Am. Chem. Soc.* **1992**, *114*, 10890−10897.
(33) (a) Bernardi, F.; Bottoni, A.; Miscione, G. P. *Organometallics* **2001**, *20*, 2751−2758. (b) Bottoni, A.; Higueruelo, A. P.; Miscione, G. P. *J. Am. Chem. Soc.* **2002**, *124*, 5506−5513. (c) Bernardi, F.; Bottoni, A.; De Vivo, M.; Garavelli, M.; Keseru, G.; Naray-Szabo, G. *Chem. Phys. Lett.* **2002**, *362*, 1−7.
(34) (a) DiLabio, G. A.; Pratt, D. A.; Wright, J. S. *Chem. Phys. Lett.* **1998**, *297*, 181−186. (b) Wright, J. S.; Johnson, E. R.; DiLabio, G. A. *J. Am. Chem. Soc.* **2001**, *123*, 1173−1183.
(35) (a) Godbout, N.; Salahub, D. R.; Andzelm, J.; Wimmer, E. *Can. J. Chem.* **1992**, *70*, 560−571. (b) *UniChem DGauss*, version 2.3.1; Cray Research, Inc.: Chippewa Falls, WI, 1994.
(36) Barone, V.; Cossi, M. *J. Phys. Chem. A* **1998**, *102*, 1995 -2001.
(37) Cossi, M.; Rega, N.; Scalmani, G.; Barone, V. *J. Comp. Chem* **2003,** *24*, 669−681.
(38) Maseras, F.; Morokuma, K. *J. Comp. Chem.* **1995**, *16*, 1170−1179.
(39) Vreven, T.; Morokuma, K.; Farkas, O.; Schlegel, H. B.; Frisch, M. J. *J. Comp. Chem* **2003**, *24*, 760−769.
(40) Wilson, III, D. M.; Takeshita, M.; Grollman, A. P.; Demple, B. *J. Biol. Chem.* **1995**, *270*, 16002−16007.
(41) Wilson, S. H.; Kunkel, T. A. *Nat. Struct. Biol.* **2000**, *7*, 176−178.
(42) Jang, Y. H.; Goddard, III, W. A.; Noyes, K. T.; Sowers, L. C.; Hwang, S.; Chung, D. S. *Chem. Res. Toxicol.* **2002**, *15*, 1023−1035.
(43) Zoltewicz, J. A.; Clark, D. F.; Sharpless, T. W.; Grahe, G. *J. Am. Chem. Soc.* **1970**, *92*, 1741−1750.
(44) Banerjee, A.; Yang, W.; Karplus, M.; Verdine, G. L. *Nature* **2005**, *434*, 612−618.
(45) Fromme, J. C.; Banerjee, A.; Huang, S. J.; Verdine, G. L. *Nature* **2004**, *427*, 652−656.
(46) Horenstein, B. A.; Parkin, D. W.; Estupiñán, B.; Schramm, V. L. *Biochemistry* **1991**, *30*, 10788−10795.
(47) Kline, P. C.; Schramm, V. L. *Biochemistry* **1993**, *32*, 13212−13219.
(48) Mentch, F.; Parkin, D. W.; Schramm, V. L. *Biochemistry* **1987**, *26*, 921−930.
(49) Xu, Y.; Grubmeyer, C. *Biochemistry* **1998**, *37*, 4114−4124.
(50) Chen, X.-Y.; Berti, P. J.; Schramm, V. L. *J. Am. Chem. Soc.* **2000**, *122*, 1609−1617.
(51) The value of the free energy activation barrier has been obtained from the experimental value of the k_{cat} using the Eyring equation.